Electrochemical versus Gas-Phase Oxidation of Ru Single-Crystal Surfaces

W. F. Lin, M. S. Zei,* Y. D. Kim, H. Over,* and G. Ertl

Fritz-Haber-Institut der Max-Planck-Gesellschaft, Faradayweg 4-6, D-14195 Berlin, Germany

Received: January 27, 2000; In Final Form: April 11, 2000

The electrochemical uptake of oxygen on a Ru(0001) electrode was investigated by electron diffraction, Auger spectroscopy, and cyclic voltammetry. An ordered (2 × 2)-O overlayer forms at a potential close to the hydrogen region. At +0.42 and +1.12 V vs Ag/AgCl, a (3 × 1) phase and a (1 × 1)-O phase, respectively, emerge. When the Ru electrode potential is maintained at +1.12 V for 2 min, RuO_2 grows epitaxially with its (100) plane parallel to the Ru(0001) surface. In contrast to the RuO_2 domains, the non-oxidized regions of the Ru electrode surface are flat. If, however, the electrode potential is increased to +1.98 V for 2 min, the remaining non-oxidized Ru area also becomes rough. These findings are compared with O overlayers and oxides on the Ru(0001) and Ru(10$\bar{1}$0) surfaces created by exposure to gaseous O_2 under UHV conditions. On the other hand, gas-phase oxidation of the Ru(10$\bar{1}$0) surface leads to the formation of RuO_2 with a (100) orientation. It is concluded that the difference in surface energy between RuO_2(110) and RuO_2(100) is quite small. RuO_2 again grows epitaxially on Ru(0001), but with the (110) face oriented parallel to the Ru(0001) surface. The electrochemical oxidation of the Ru(0001) electrode surface proceeds via a 3-dimensional growth mechanism with a mean cluster size of 1.6 nm, whereas under UHV conditions, a 2-dimensional oxide film (1−2 nm thick) is epitaxially formed with an average domain size of 20 μm.

1. Introduction

Both ruthenium and ruthenium dioxide (RuO_2) are important electrode materials in electrocatalysis.[1] Whereas Ru-modified Pt electrodes are considered to be promising candidates for low-temperature fuel cell applications,[2−4] RuO_2 is an efficient material for the electrooxidative generation of Cl_2 and O_2 and for its resistance against such aggressive chemicals.[5] Additional applications of RuO_2 include its use in the partial oxidation of hydrocarbons[6] and as new-generation contacts/interconnects in Si devices.[7] The activity and selectivity of Ru oxides depend largely on the oxidation state of the metal, with different ruthenium oxides exhibiting distinct physical and catalytic properties.[1] The interaction between ruthenium and oxygen has, therefore, been the subject of extensive investigation, which is well documented for the chemisorption of oxygen on ruthenium single crystals prepared under ultrahigh vacuum (UHV) conditions.[8−16]

Recently, oxygen-rich Ru(0001) surfaces have been shown to be very active for the conversion of CO to CO_2, even under UHV conditions where the pure or adsorbed-oxygen-covered Ru(0001) surfaces are virtually inactive.[17,18] The Ru(0001) surface was oxidized by exposure to large amounts of molecular oxygen at elevated sample temperatures (600−800 K). The active parts of such oxygen-rich phases were identified with RuO_2, which grows epitaxially on Ru(0001) with its (110) face oriented parallel to Ru(0001).[19] As for the case of Ru(0001), the Ru(10$\bar{1}$0) surface can be oxidized by oxygen exposure, leading to the epitaxial growth of the RuO_2, this time, however, along (100) orientation.

Ruthenium can also be oxidized electrochemically, transforming the Ru electrode into a RuO_2-covered electrode.[20−29] So far, little work has been performed on the electrooxidation of single-crystal Ru surfaces.[30,31] In this paper, we describe the electrochemical route for preparing RuO_2 films on Ru(0001) electrodes and compare the properties of such films with those of RuO_2 films grown under UHV conditions. We report on a voltammetric study of a well-defined Ru(0001) electrode and the epitaxial growth of RuO_2(100) on Ru(0001) in 0.1 M $HClO_4$ in a potential range between 1.10 and 1.98 V vs Ag/AgCl. In particular, data from reflection high-energy electron diffraction (RHEED) were evaluated to analyze the structure and orientation of RuO_2 on the Ru(0001) substrate.

2. Experimental Section

The experiments were conducted in a UHV-EC system that consists of a main UHV chamber (base pressure, $<2 \times 10^{-10}$ mbar), an electrochemical chamber (EC) (base pressure less than 9×10^{-10} mbar), and an electrochemical cell together with a closed sample-transfer system.[32,33] The main chamber houses instruments for low-energy electron diffraction (LEED), reflection high-energy electron diffraction (RHEED), and Auger electron spectroscopy (AES). The electrochemical section consists of two cells. We used a flow-cell procedure, which allows us to change electrolyte solutions under potential control and in an air-free atmosphere.[33]

RHEED experiments were performed with an incident electron beam energy of 40 keV and at grazing incidence of 1−2°. The RHEED electron beam also served as the primary electron source for AES experiments. This combination allows for RHEED and AES measurements to be recorded from the same surface region, thus correlating structure and composition data.

The working electrode, a Ru(0001) single-crystal disk of 7.5-mm diameter and 2-mm thickness, was clamped between two

* Authors to whom correspondence should be addressed. Fax: ++49-30-84135106. E-mail: zei@fhi-berlin.mpg.de, over@fhi-berlin.mpg.de.

10.1021/jp0003149 CCC: $19.00
Published on Web 06/03/2000

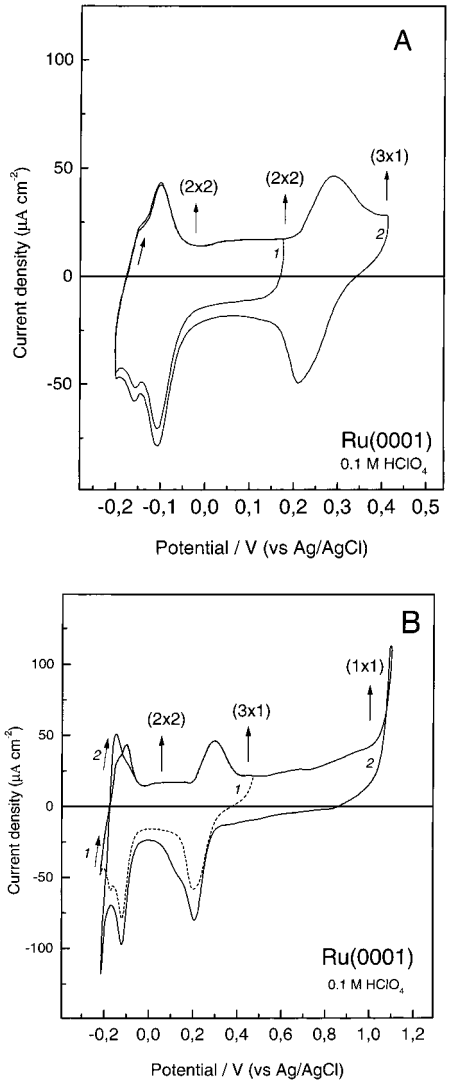

Figure 1. Cyclic voltammograms for a Ru(0001) electrode in 0.1 M $HClO_4$ solution. Anodic potential limits are **(A)** 0.42 and **(B)** 1.12 V vs Ag/AgCl. Resulting LEED patterns are indicated when the sample was emersed at the particular polarization. The sweep rate is 50 mV/s.

tungsten wires, which were also used for resistive heating of the sample. The electrode surface was prepared by cycles of argon ion sputtering (5×10^{-5} mbar, room temperature and 600 °C) and hydrogen treatment (5×10^{-7} mbar, 600 °C), which were followed by high-temperature (above 1000 °C) annealing, until AES and LEED/RHEED data indicated a clean and well-ordered surface. The UHV-prepared Ru(0001) electrode was then transferred to the electrochemical chamber, which was subsequently floated by 5.0 N argon gas. Nitrogen overpressure efficiently kept air out of the transfer system at all stages of the experiments. The glass capillary, filled with an aqueous electrolyte of 0.1 M $HClO_4$ in a 5.0 N nitrogen atmosphere, was passed through a gate valve from its lower idle position into the electrochemical chamber. The electrode surface was then allowed to contact the solution via a meniscus configuration and under potential control. Millipore water (>18 MΩ) and suprapure-grade perchloric acid $HClO_4$ (Merck) were used for the electrolyte. All experiments were performed at room temperature, and all potentials are given vs the Ag/AgCl electrode in saturated KCl solution. The UHV-prepared Ru(0001) electrode was subjected to potential cycling in the $HClO_4$ solution in a defined potential range. The electrochemical data were recorded, and the related surface structure of the emersed

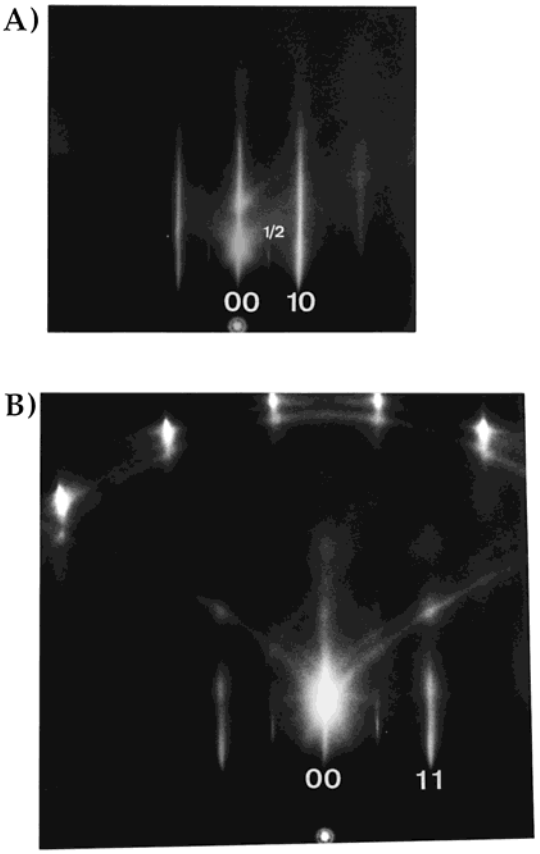

Figure 2. (2 × 2) RHEED pattern along the (A) [1000] and (B) [10$\bar{1}$0] directions of a Ru(0001) electrode after potential cycling between −0.2 and 0.2 V vs Ag/AgCl and emersion at 0.2 V. The electrolyte is 0.1 M $HClO_4$. The sweep rate is 50 mV/s.

Ru electrode could subsequently be characterized ex situ by LEED/RHEED and AES techniques. After the electrochemical experiments, the electrode was tilted close to vertical position in order to facilitate solution draining to the edge of the surface, where the drop was stripped off via a thin Teflon tubing attached to a syringe (dry emersion). Finally, the electrochemical cell was withdrawn to its original lower position. After the gate valve was closed, the electrochemical chamber was evacuated to 10^{-7} mbar before the sample was quickly transferred back into the main UHV chamber for surface characterization.

In a second chamber, the Ru(0001) sample was exposed to various O_2 doses. The second UHV chamber[34] is equipped with 4-grid back-view LEED optics, instruments for Auger electron spectroscopy (AES) and thermal desorption spectroscopy (TDS), and facilities for the cleaning and preparation of the Ru surfaces. The sample temperature could be varied from 100 K (by cooling with liquid N_2) to 1530 K (by direct resistive heating). The LEED intensities as a function of the incident energy of the electrons were collected at normal incidence of the primary beam while the sample temperature was maintained at 100 K. A computer-controlled video camera was used to record spot intensities from the LEED fluorescence screen. As shown in a previous communication, an exposure of about 10^6 L of O_2 (sample temperature, 600−700 K) results in a surface that consists of RuO_2(110) epitaxially grown on Ru(0001) coexisting with patches of chemisorbed (1 × 1)-O phases.[19] Similar experiments were conducted with a Ru(10$\bar{1}$0) sample on which the epitaxial growth of RuO_2 was again observed, but this time with the (100) orientation parallel to the Ru(10$\bar{1}$0) surface. Both the Ru(0001) and the Ru(10$\bar{1}$0) samples were cleaned by argon ion bombardment at 1 keV followed by cycles of oxygen

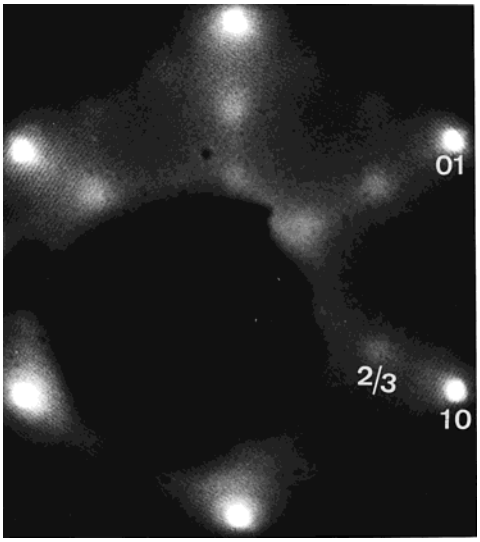

Figure 3. (3 × 1) LEED pattern (57 eV) of a Ru(0001) electrode after potential cycling between −0.2 and 0.42 V vs Ag/AgCl and emersion at 0.42 V. The electrolyte is 0.1 M $HClO_4$. The sweep rate is 50 mV/s.

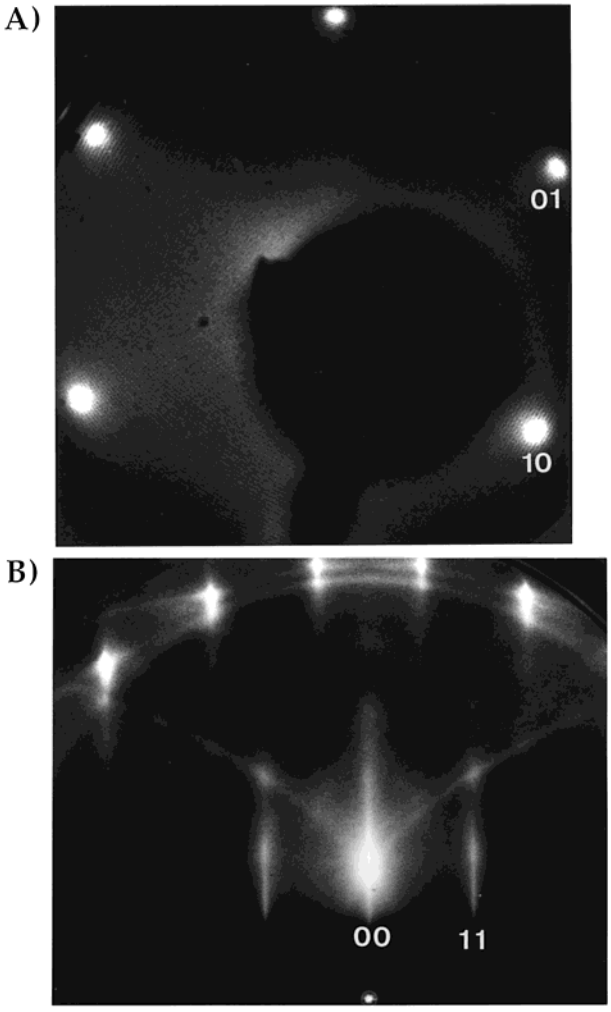

Figure 4. (A) (1 × 1) LEED pattern (60 eV) and **(B)** (1 × 1) RHEED pattern along the [10$\bar{1}$0] direction of a Ru(0001) electrode after potential cycling between −0.2 and 1.12 V vs Ag/AgCl and emersion at 1.06 V. The electrolyte is 0.1 M $HClO_4$. The sweep rate is 50 mV/s.

adsorption and thermal desorption in order to remove surface carbon. Final traces of oxygen were removed by heating the surface to 1530 K, resulting in sharp (1 × 1) LEED patterns and no impurity detected in AES spectra.

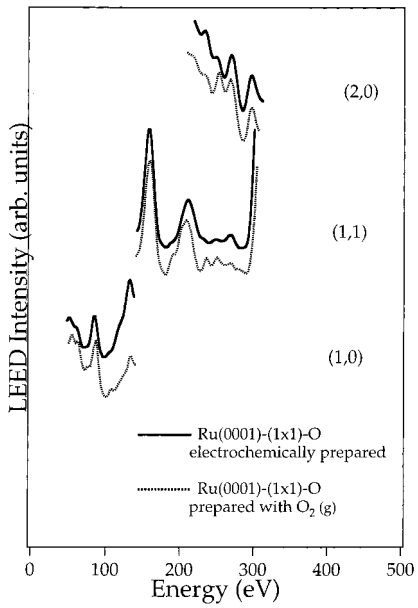

Figure 5. Comparison of LEED I/V curves of the (1 × 1) phase prepared by immersing the Ru(0001) electrode at 1.06 V with those of a well-defined Ru(0001)-(1 × 1)-O surface that was prepared under UHV conditions. The striking similarity between these data sets (as quantified by a Pendry *r*-factor of 0.06) indicates identical surface structures.

3. Results and Discussion

Figure 1a shows cyclic voltammograms from the UHV-prepared Ru(0001) electrode in a 0.1 M $HClO_4$ solution, as the potential sweeps between −0.2 and +0.4 V vs Ag/AgCl. Two characteristic anodic/cathodic peaks at −0.1 and +0.29 V are observed. In the potential range between −0.2 and 0 V, the voltammogram is dominated by a current peak at −0.1 V, which is characteristic for the H adsorption/desorption at the Ru surface. The current peak at −0.1 V does not change upon cycling of the potential, as long as the potential does not exceed +0.2 V. However, the intensity of the reduction peak increases markedly after anodic sweeping to +0.4 V, as shown in curve 2 of Figure 1a, which indicates additional oxygen uptake, as will be further outlined below. The voltammetric profile shown in Figure 1a for H adsorption/desorption in 0.1M $HClO_4$ is quite similar to that obtained by Cao et al.[30] for a Ru(0001) electrode in 0.01 M KF. The latter indicates a cathodic potential shift of 200 mV compared to our data. This may be related to the different pH value and different kind of electrolyte.

To gain information about the surface structure, composition, and morphology, we emersed the Ru(0001) electrode at certain potential values after cyclic potential sweeps and investigated the resulting surfaces ex situ by LEED, RHEED, and AES techniques. Figure 2a and b shows (2 × 2) RHEED patterns (for two azimuths) of the Ru(0001) electrode after potential cycling between −0.2 V and +0.2 V and emersion of the sample at +0.2 V. The LEED pattern (not shown) exhibits only faint half-order spots. The corresponding AES spectrum reveals an O Auger signal, suggesting that the (2 × 2) structure arises from an oxygen overlayer. A similar interpretation was put forward by Cao et al.[30]

When the anodic sweep limit was extended to +0.415 V, an anodic current peak at +0.3 V and a cathodic peak at +0.2 V appeared. After such a potential cycling, a (3 × 1) superstructure

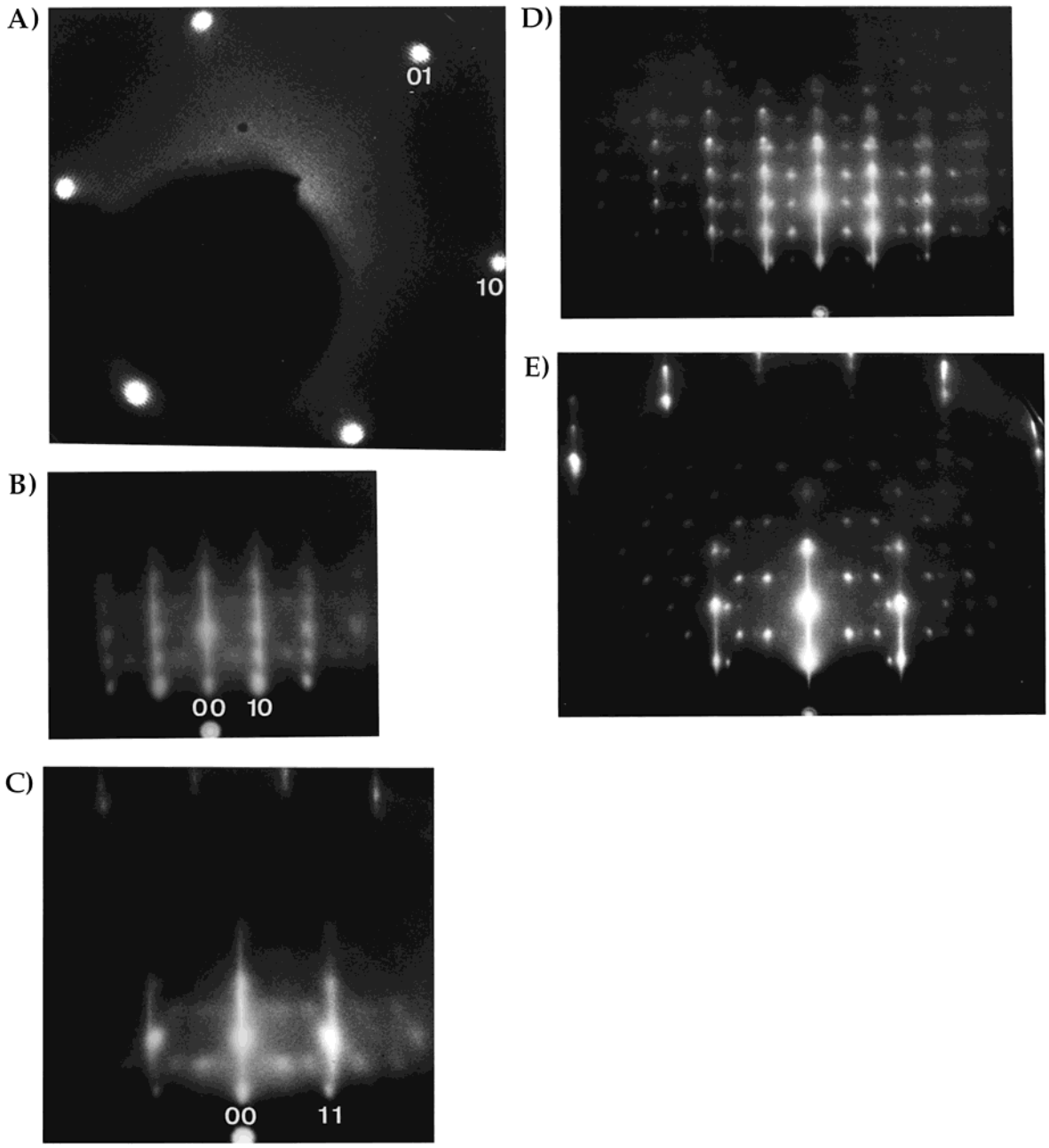

Figure 6. LEED and RHEED patterns of a Ru(0001) electrode after potential cycling between −0.2 and 1.12 V vs Ag/AgCl, potential maintenance at 1.12 V for 2 min, and emersion at 1.06 V. **(A)** The LEED pattern is a (1 × 1), whereas the RHEED patterns along the (B) [1000] and (C) [10$\bar{1}$0] azimuths show additional 3D reflections that belong to RuO_2(100). RHEED patterns along the (D) [1000] and (E) [10$\bar{1}$0] azimuths after the electrochemically prepared surface is annealed at 700 K for 11 min in UHV. The electrolyte is 0.1 M $HClO_4$. The sweep rate is 50 mV/s.

appeared in the LEED data when the Ru electrode surface was emersed at 0.415 V (cf. Figure 3). This phase cannot be produced by exposure of Ru(0001) to gaseous O_2 under UHV conditions. The composition for the (3 × 1) phase is, therefore, not clear at the moment. It might be that this surface structure is formed by the adsorption of O and OH. The electric charge measured between 0.2 and 0.4 V after correction for the double-layer charging current gives a charge value of 75 μC/cm^2, which is close to $^1/_3$ ML coverage (83 μC/cm^2) and, therefore, consistent with a (3 × 1)-O overlayer. We found the corresponding reduction peak at 0.2 V, which is in accordance with the reduction peak at −0.08 V found by Cao et al.[30] in 0.01 M KF solution, considering the cathodic potential shift of 200 meV.

When the Ru(0001) electrode was subjected to three cycles of anodic and cathodic sweeps up to +1.12 V (Figure 1b), the corresponding cathodic peak became significantly broader. The anodic peak at 0.3 V was still discernible. The cyclic voltammogram in Figure 1b shows that the cathodic feature at 0.2 V overlaps with the reduction peak of the new oxygen species. The Ru electrode surface exhibits a (1 × 1)-phase LEED/RHEED pattern upon potential cycling up to 1.12 V and emersion at 1.06 V (cf. Figure 4a and b). The AES spectrum indicates that the O coverage in this (1 × 1) phase is much higher than that for the (2 × 2)-O. It is interesting to note that the electrochemically prepared (1 × 1) phase is very similar to that obtained by gas-phase oxidation of Ru(0001) under UHV conditions.[10] This was corroborated by a comparison of experimental LEED I/V data taken from the (1 × 1) phase generated by O electrosorption at 1.06 V with those of the UHV-prepared Ru(0001)-(1 × 1)-O phase (cf. Figure 5). The striking similarity of the LEED I/V curves indicates that the local adsorption geometries must be the same,[35] and therefore, the

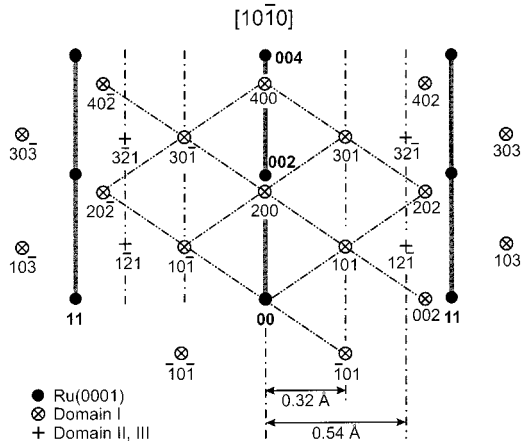

Figure 7. Schematic presentation of the RHEED pattern from Figure 6 including the proper indexing according to a structure-factor analysis, assuming the three rotational domains of $RuO_2(100)$ grown on Ru(0001).

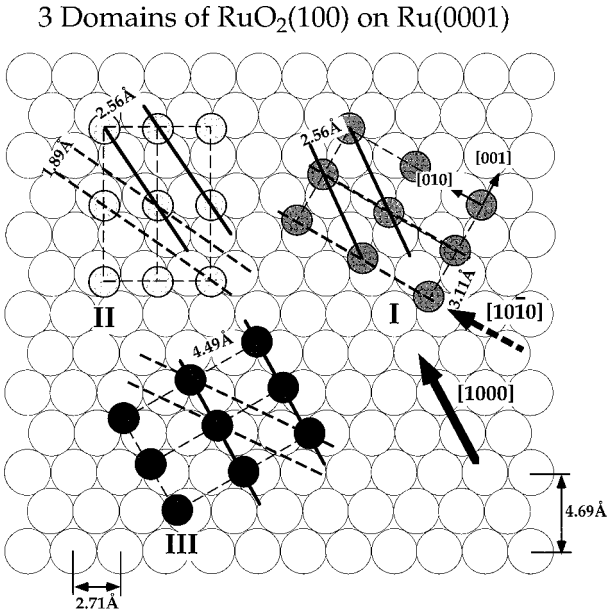

Figure 8. Schematic representation of the three rotational domains of $RuO_2(100)$ on Ru(0001) with the [001] and [010] directions aligned along the [1000] and [10$\bar{1}$0] directions of the Ru(0001) substrate. Important distances between atomic rows of $RuO_2(100)$ are indicated.

electrochemically prepared (1 × 1) phase is identified with a (1 × 1)-O overlayer. The 2-dimensional (2D) reflection streaks in the RHEED data (Figure 4b) demonstrate that the Ru(0001)-(1 × 1)-O electrode surface is still flat even after anodic/cathodic sweeps up to 1.12 V. This result differs from that for a Pt(111) electrode for which a rough surface was obtained after the same potential cycling to the oxidation region.[36]

An even higher oxygen load was achieved by holding the Ru electrode at +1.12 V for 2 min. This procedure was accompanied by a drastic increase in the oxygen signal in the AES spectrum, consistent with oxide formation or oxygen dissolution in the Ru bulk. The corresponding LEED pattern in Figure 6a still shows a (1 × 1) array of spots similar to that shown in Figure 4a, although the LEED spots are significantly broader. On the other hand, the RHEED pattern (Figure 6b and c) for the same sample surface indicates 3-dimensional (3D) spots, in addition to the (1 × 1) streaks, which are assigned to small $RuO_2(100)$ clusters, as shown below. A much better RHEED pattern with very sharp 3D spots could be obtained by annealing the surface in UHV to 800 K for 5 min (cf. Figure 6d and e); at 800 K, no oxygen from the oxide is desorbing.[17] For the sake of clarity, the reciprocal lattice net for the corresponding RHEED patterns obtained at a [10$\bar{1}$0] direction of the incident electron beam are sketched in Figure 7. From the width of the 3D RHEED spots, the average oxide cluster size is estimated to be about 1.6 nm. Altogether, it seems that the electrooxidation of Ru(0001) proceeds via a "nucleation and growth" type of mechanism, which may be supported by the measurement of current transients. In addition, as for the gas-phase oxidation, the onset of oxidation sets in only when the Ru(0001) surface is covered by a complete (1 × 1)-O overlayer. Obviously, the (1 × 1)-O overlayer serves as a required precursor state for the subsequent oxidation process.

A simple approach for determining the in-plane lattice constants related to these 3D spots is the following. We first draw lines through all of the spots, which line up in the perpendicular direction (parallel to the reflection streaks). The distance from the (00) streak to these 3D-related lines in conjunction with the distance between the (00) streak and the next substrate streak [0.467 $Å^{-1}$ for the (10) streak and 0.739 $Å^{-1}$ for the (11) streak] provide promising candidates for reciprocal lattice vectors of the surface Ru oxide. In the [10$\bar{1}$0] direction, these values are 0.32 and 0.54 $Å^{-1}$, which are associated with real lattice constants of 3.12 and 1.86 Å, respectively (cf. Figure 8). Analogously, in the [1000] direction we derived values of 0.222 and 0.391 $Å^{-1}$, which are related to real lattice constants of 4.50 and 2.56 Å, respectively. The values 3.12 Å and 4.50 Å agree almost perfectly with the dimension of the $RuO_2(100)$ unit cell (3.11 Å × 4.49 Å). Furthermore, the $RuO_2(100)$ film is aligned with its short axis along the [1000] direction of Ru(0001). When a $RuO_2(100)$ film is grown on Ru(0001), then on the basis of symmetry [2-fold axis of $RuO_2(100)$ vs 3-fold axis of Ru(0001)], three rotational domains of $RuO_2(100)$ exist on the substrate surface (rotated by 120°). These domains are plotted in Figure 8. If the RHEED beam is aligned along the [10$\bar{1}$0] direction, then distances between atomic rows of RuO_2 that are perpendicular to the scattering plane become visible in the RHEED pattern, e.g., a distance of 3.11 Å for domain I and a distance of 1.85 Å for domains II and III (cf. solid lines in Figure 8). These are exactly the distances derived from the RHEED pattern along the [10$\bar{1}$0] azimuth. Analogously, in the [1000] direction, an atomic row distance of 4.49 Å for domain III and a distance of 2.56 Å for domains I and II should be seen in the RHEED pattern, as is, indeed, experimentally verified. From the vertical distance between the 3D spots in the RHEED pattern ([10$\bar{1}$0] azimuth), the layer spacing between equivalent (100) planes of RuO_2 was determined to be 4.50 Å, which is close to the corresponding bulk value of 4.49 Å for $RuO_2(100)$. Altogether, this provides very strong evidence that RuO_2 is grown on Ru(0001) with its (100) orientation parallel to the Ru(0001) surface. The epitaxial growth of RuO_2 clusters on the Ru(0001) electrode found here is in nice agreement with previous XPS measurements of electrooxidized Ru.[37]

In a more elaborate analysis, the 3D reflections of RuO_2 are indexed on the basis of a kinematic structure factor calculation[38] (cf. Table 1). With these structure factors, we are also able to explain the systematic absence or the low intensity of particular reflections in the RHEED data. For instance, the (100), (001), and (102) reflections have zero structure factors and are also not observed in the experimental RHEED pattern (cf. Figures 6b and 7). From the reciprocal lattice analysis, the existing and missing 3D reflections in the RHEED pattern can be unequivocally assigned to the three rotational domains of $RuO_2(100)$ with

TABLE 1: Kinematic Structure Factors of RuO_2 with *h* and *k* in the *a Direction and *l* in the *c** Direction**

h	*k*	*l*	length ($Å^{-1}$)	structure factor
1	0	0	0.222	0
0	1	0	0.222	0
0	1	1	0.391	3655
1	1	0	0.314	5799
1	1	1	0.450	305
2	1	1	0.592	3469
2	1	0	0.497	121
2	0	0	0.445	2411
3	1	0	0.703	2021
0	0	1	0.322	0
0	0	2	0.644	4307
1	0	1	0.391	3655
0	1	2	0.681	0
1	0	2	0.681	0
2	0	0	0.445	2411
2	0	2	0.782	1330
3	0	1	0.740	3200

[a] Several structure factors are quite small because of the centrosymmetry of the Ru sublattice and the fact that Ru is a much stronger scatterer than O.[38]

its [100] direction aligned along the [10$\bar{1}$0] direction of the Ru(0001) substrate surface (cf. Figure 8).

The observation of both the (1 × 1) streak and the 3D spots of RuO_2 indicates that the non-oxidized Ru(0001) surface is still flat and that the only rough areas are those where RuO_2 clusters are formed. We should note that the total oxygen uptake of the Ru(0001) electrode increases monotonically with time while the potential is maintained at +1.12 V in $HClO_4$.

It is quite remarkable that the epitaxial growth of RuO_2(100) on Ru(0001) in a $HClO_4$ electrolyte differs profoundly from that resulting from the exposure of 10^6 L of O_2 to Ru(0001) at a sample temperature of 700 K under UHV conditions.[17] For the latter preparation method, RuO_2 domains grow epitaxially with the (110) face parallel to the Ru(0001) surface.[19] The LEED pattern of RuO_2(110) on Ru(0001) is shown in Figure 9a together with a sketch of the diffraction spots in Figure 9b. The LEED pattern is attributed to the superposition of three (120°) rotational domains of RuO_2(110) (cf. Figure 10), and the hexagonal array of reflections originates from additional patches of a (1 × 1)-O overlayer. We also show a hypothetical LEED pattern of RuO_2(100) on Ru(0001) (cf. Figure 9c). From a comparison of parts b and c of Figure 9, it is clear that the LEED data allow us to discriminate readily between RuO_2(110) and RuO_2(100) domains. The LEED patterns in Figure 9a and b indicate that RuO_2 grows epitaxially on Ru(0001), i.e., the RuO_2(110) lattice has a well-defined orientation with respect to the substrate lattice. Because the RuO_2(110) overlayer structure is incommensurate with the underlying substrate, i.e., the combination of the RuO_2(110) and the substrate lattices does not produce a finite unit cell that is simply related to the substrate lattice, the oxide film is presumably unstrained. From STM images, the averaged RuO_2(110) domain size was determined to be some 20 μm, and the thickness was about 1−2 nm, in accordance with recent X-ray reflectivity.[19]

The atomic geometry of the RuO_2(110) film on Ru(0001) was determined by LEED measurements and DFT calculations.[19] Briefly, the oxide surface turned out to be a bulk-truncated RuO_2(110) surface, which is terminated with bridging oxygen rows. Because of the presence of bridging oxygen rows above the main surface plane, one-half of the surface Ru atoms are only 5-fold coordinated with O atoms and the other half are 6-fold coordinated (cf. Figure 11). The Ru−O bond lengths in bulk RuO_2 are 1.91 and 2.01 Å. The bridging O atoms were found to be 1.17 Å above the outermost Ru atoms, leading to a Ru−O bond length of 1.93 Å. The underlying mixed Ru−O layer is buckled by 0.20 Å. The layer distance between the O subplane of the topmost Ru + O layer and the underlying O bilayer is expanded by about 0.1 Å. All other structural parameter values are close to distances known from bulk RuO_2(110).

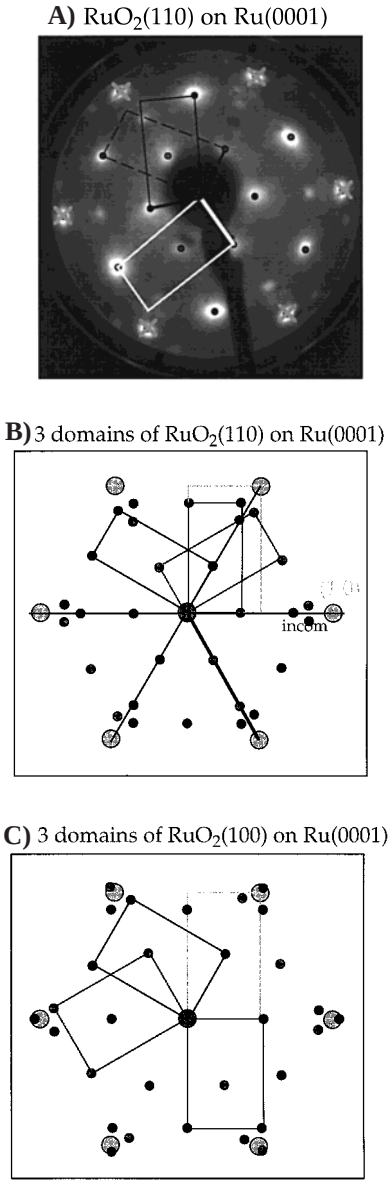

Figure 9. (A) LEED pattern of the oxygen-rich Ru(0001) surface (with 10 ML of oxygen), $E = 63$ eV, $T = 110$ K. It consists of a (1 × 1) hexagonal pattern (indicated by crosses) and a superposition of three (1 × 1) rectangular patterns rotated by 120° that belong to RuO_2(110) domains. **(**B**)** Schematic LEED pattern of three rotational RuO_2(110) domains on Ru(0001) that are aligned along the [10$\bar{1}$0] direction. **(**C**)** Schematic LEED pattern of three rotational RuO_2(100) domains on Ru(0001) that are aligned along the [10$\bar{1}$0] direction.

The same gas-phase preparation procedure applied to Ru(10$\bar{1}$0) leads, however, to the epitaxial growth of RuO_2(100), as documented by the 0.86 × 1 LEED pattern shown in Figure 12b. For comparison, in Figure 12a the LEED pattern of the Ru(10$\bar{1}$0)-(1× 2)-4O structure is also depicted. This phase is considered as the initial stage of the oxidation process of Ru(10$\bar{1}$0). At lower O coverages of 0.5 and 1.0 ML, c(2 × 4)-2O and (2 × 1)-p2mg-2O overlayer structures, respectively, can be formed on Ru(10$\bar{1}$0). [16] Along the [0001] direction, the

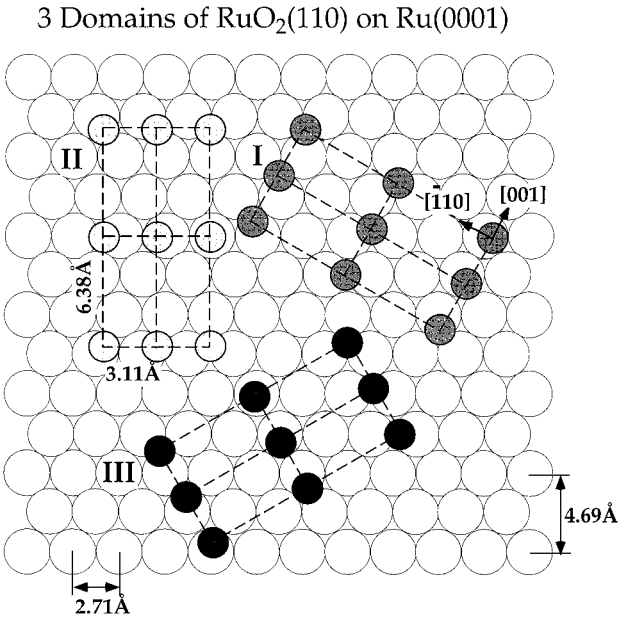

Figure 10. Schematic of the three rotational domains of RuO_2(110) on Ru(0001) with the [001] and [$\bar{1}$10] directions aligned along the [1000] and [10$\bar{1}$0] directions of the Ru(0001) substrate.

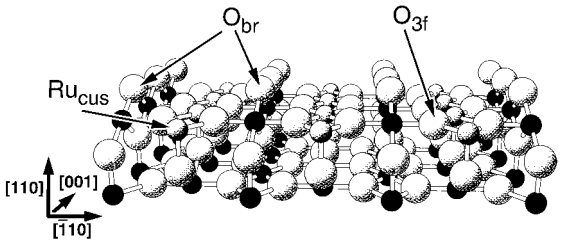

Figure 11. Ball-and-stick model of the bridging-oxygen-terminated RuO_2(110) surface. Large balls represent oxygen, and small balls represent ruthenium atoms of RuO_2(110). A highly active coordinatively unsaturated Ru atom (Ru_{cus}) as well as bridge-bonded and 3-fold coordinated O atoms are indicated by arrows.

RuO_2(100) is matched with the Ru(10$\bar{1}$0) substrate, although the lattice misfit along the long axis of RuO_2(100) is 4.5% [4.28 Å on Ru(10$\bar{1}$0) vs 4.49 Å in RuO_2(100)]. This implies that the RuO_2(100) is unidirectionally strained, quite in contrast to the case of Ru(0001) for which the RuO_2(110) film is incommensurate with respect to the underlying substrate. From these findings, one can conclude that the difference between the surface energies of RuO_2(100) and RuO_2(110) is only marginal, and therefore, strain energy and kinetic considerations are important factors governing the actual growth mode.

Probably even more important is the actual oxidation step under electrochemical conditions,[39] which may differ largely from the gas-phase oxidation. Electrooxidation in acidic solution takes place via adsorption of H_2O on the electrode surface. The adsorbed H_2O molecule may fall apart into OH and H^+ or O and 2 H^+ by charge transfer, with the H^+ ions going into solution. This process might be followed by a place exchange between OH or O and the surface metal atoms and an ensuing electron transfer to form the oxide. Further oxidation may be inhibited by the high conductivity[40] of RuO_2, which cannot sustain a high electric field across the oxide film to ensure electromigration of OH^-, O^-, and metal ions through the oxide film. Because we already saw that a (1 × 1)-O overlayer seems to serve as a necessary precursor for the subsequent oxidation step (both in electrochemical and gas-phase environment), we favor the adsorption of O and exchange with Ru rather than the participation of adsorbed OH in the actual oxidation process.

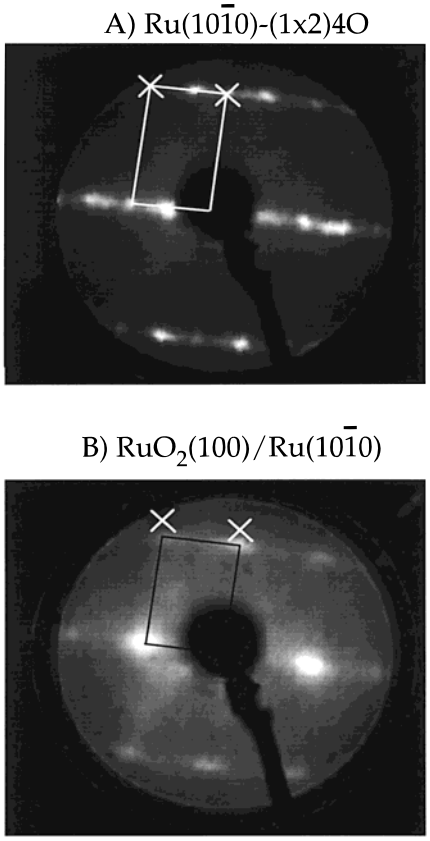

Figure 12. (A) LEED pattern of the Ru(10$\bar{1}$0)-(1 × 2)-4O overlayer phase. (B) LEED pattern of RuO_2(100) that is grown epitaxially on Ru(10$\bar{1}$0), with $E = 63$ eV, $T = 110$ K.

In the following, we compare our preparation routes with alternative procedures for ruthenium dioxide formation reported in the literature. For instance, the epitaxial growth of RuO_2 by metal-organic chemical vapor deposition results in a RuO_2 film with its (110) orientation parallel to MgO(100), whereas on $LaAlO_3$(100), the RuO_2 film grows with its (100) orientation parallel to the surface.[41] Strain was considered to be responsible for the different growth orientation. The growth of RuO_2 films on glass or sapphire by reactive sputtering was found to proceed preferentially in the (110) orientation.[42,43] It is quite interesting that the growth of RuO_2 by reactive sputtering differs markedly between Pt(111) and Ru(0001) substrates. Whereas on Pt(111), RuO_2 grows with the (100) orientation parallel to the substrate surface, on Ru(0001), RuO_2 grows with the (110) orientation or with a mixture of (110) and (100) orientations along the substrate surface.[44]

It is important to recall that electrooxidation of Ru(0001) (by water) was performed at room temperature, whereas oxidation with dry O_2 requires elevated temperatures (600−800 K). Therefore, it is conceivable that, because of kinetic limitations, only small RuO_2 grains with mean diameters <2 nm can grow in electrochemical environments and at low temperature, whereas larger areas of RuO_2 with average 2D sizes of 20 μm and a thicknesses of 1−2 nm are formed at higher temperatures under UHV conditions. The cluster size of the electrochemically prepared RuO_2 was derived from the full width of half-maximum of the RHEED spots, whereas the size of UHV-grown RuO_2 was determined by STM measurements.

To investigate the growth of the surface oxide at even higher electrode potentials, the positive potential limit in the anodic

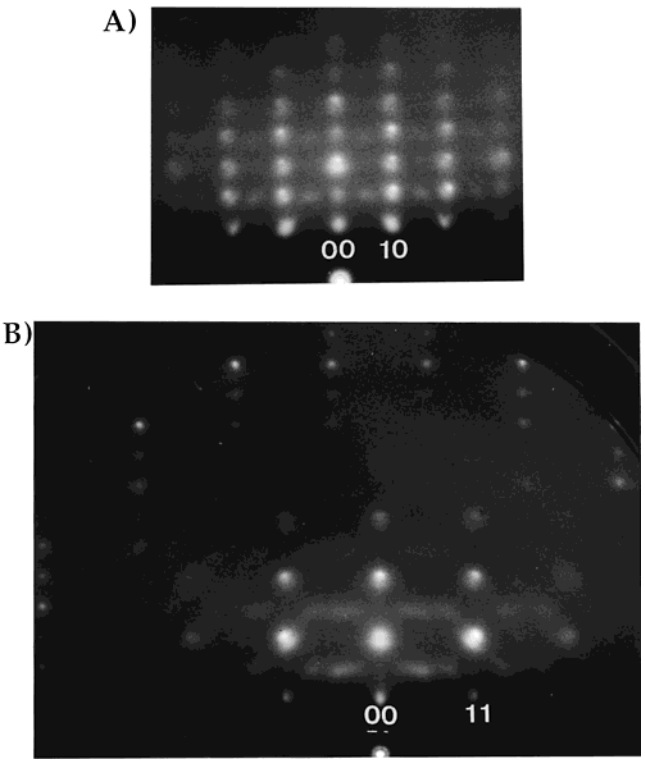

Figure 13. RHEED patterns of a Ru(0001) electrode after potential cycling between −0.2 and 1.98 V vs Ag/AgCl, potential maintenance at 1.98 V for 21 min, and emersion at 1.98 V. The RHEED patterns along the (A) [1000] and (B) [10$\bar{1}$0] azimuth show, in addition to the RuO_2(100)-related 3D spots, substrate-related 3D spots. The electrolyte is 0.1 M $HClO_4$. The sweep rate is 50 mV/s.

sweep was increased to 1.98 V, at which the electrode is known to dissolve with formation of RuO_4 and O_2.[45] Therefore, the found growth of RuO_2(100) on Ru(0001) is quite surprising. The RHEED patterns for the Ru electrode emersed at 1.98 V are reproduced in Figure 13. The formerly streaky 2D (1 × 1) RHEED reflections of the substrate are replaced by 3D spots, indicating that now the Ru surface is also rough. The other 3D spots of the RHEED pattern are due to RuO_2(100), whose mean cluster size is about 1.6 nm. A plausible interpretation is that, under such conditions, a high density of RuO_2 clusters is produced, and between the RuO_2 clusters, only small areas of Ru patches are left, which, in turn, can be regarded as small Ru clusters.

Finally, it must be emphasized that the structural characterization of the electrochemically synthesized RuO_2(100) phase on Ru(0001) could only be achieved by RHEED, but not by LEED, experiments. The failure of LEED measurements to detect diffraction spots related to the electrochemically prepared RuO_2(100) on Ru(0001) may be because of the rough surfaces of the small RuO_2(100) clusters, whereas the whole volume of the RuO_2(100) clusters contributes to the RHEED 3D reflection intensity. In addition, the 3D reflections of RHEED suffered only from a small momentum transfer perpendicular to the RuO_2(100) surface so that the sensitivity to vertical roughness of the oxide surfaces is less severe than that with LEED, where the momentum transfer perpendicular to the surface is large, thus preventing reliable LEED observations.

4. Summary

We investigated the electrochemical uptake of oxygen on a Ru(0001) electrode by LEED/RHEED, AES, and cyclic voltammetry techniques. An ordered (2 × 2)-O overlayer forms on the Ru(0001) at a potential close to the hydrogen region. At +0.42 and +1.12 V vs Ag/AgCl, a (3 × 1) phase with unknown composition and a (1 × 1)-O overlayer, respectively, emerged. In contrast to the (2 × 2)-O and the (1 × 1)-O overlayers, the (3 × 1) phase cannot be produced by gaseous oxygen exposure under UHV conditions. When the Ru electrode potential is maintained at +1.12 V for 2 min, 3D RuO_2 clusters grow epitaxially with their (100) orientation along the Ru(0001) surface. The mean size of these clusters is 1.6 nm. The nonoxidized Ru(0001) electrode is still flat. It seems that electrochemical oxidation proceeds via a "nucleation and growth" type of mechanism and that the (1 × 1)-O overlayer serves as a precursor for the actual oxidation process. When the electrode potential is stepped up to +1.98 V for 2 min, the complete Ru surface becomes rough. These findings are compared with those for RuO_2 layers formed on the Ru(0001) and Ru(10$\bar{1}$0) surfaces by exposure to gaseous O_2 under UHV conditions. RuO_2 also grows epitaxially as a 2D oxide film on Ru(0001), but with the (110) face oriented parallel to the Ru(0001) surface. The mean domain size is about 20 nm, and the film thickness is about 1−2 nm. On Ru(10$\bar{1}$0), however, RuO_2 grows epitaxially along the (100) orientation.

Acknowledgment. W.F.L. is grateful to the Max-Planck-Gesellschaft for a Research Fellowship. We thank W. Vogel and W. Moritz for fruitful discussions.

References and Notes

(1) Seddon, E. A.; Seddon, K. R. *The Chemistry of Ruthenium*; Elsevier Science: New York, 1984.
(2) Lee, C. E.; Bergens, S. H. *J. Electrochem. Soc*. **1998**, *145*, 4182.
(3) Ralph, T. R. *Platinum Met. Rev*. **1997**, *41*, 102.
(4) Munk, J.; Christensen, P. A.; Hammnett, A.; Skou, E. *J. Electroanal. Chem*. **1996**, *401*, 215.
(5) Mills, A. *Chem. Soc. Rev*. **1989**, *18*, 285.
(6) Ashcroft, A. T.; Cheetham, A. K.; Foord, J. S.; Green, M. L. H.; Grey, C. P.; Murrell, A. J.; Vernon, P. D. F. *Nature* **1990**, *344*, 319.
(7) Gao, Y.; Bai, G.; Liang, Y.; Dunham, G. C.; Chambers, S. A. *J. Mater. Res*. **1997**, *12*, 1844 and references therein.
(8) Madey, T. E.; Engelhardt, H. A.; Menzel, D. *Surf. Sci*. **1975**, *48*, 304.
(9) Fuggel, J. C.; Madey, T. E.; Steinkilberg, M.; Menzel, D. *Chem. Phys. Lett*. **1975**, *33*, 233.
(10) (a) Pfnür, H.; Held, G.; Lindroos, M.; Menzel, D. *Surf. Sci*. **1989**, *220*, 43. (b) Lindroos, M.; Pfnür, H.; Held, G.; Menzel, D. *Surf. Sci*. **1989**, *222*, 451.
(11) Over, H. *Prog. Surf. Sci*. **1998**, *58*, 249 and references therein.
(12) He, P.; Jacobi, K. *Phys. Rev. B* **1997**, *55*, 4751.
(13) Stampfl, C.; Schwegmann, S.; Over, H.; Scheffler, M.; Ertl, G. *Phys. Rev. Lett*. **1996**, *77*, 3371 and references therein.
(14) Mitchell, W. J.; Wang, Y.; Schick, M.; Weinberg, W. H. *J. Chem. Phys*. **1995**, *102*, 8185.
(15) Malik, I. J.; Hrbek, J. *J. Vac. Sci. Technol. A* **1992**, *10*, 2565.
(16) Schwegmann, S.; Seitsonen, A. P.; De Renzi, V.; Dietrich, H.; Bludau, H.; Gierer, M.; Over, H.; Jacobi, K.; Scheffler, M.; Ertl, G. *Phys. Rev. B* **1998**, *57*, 15487.
(17) Böttcher, A.; Niehus, H.; Schwegmann, S.; Over, H.; Ertl, G. *J. Phys. Chem*. **1997**, *101*, 11185.
(18) Böttcher, A.; Rogozia, M.; Niehus, H.; Over, H.; Ertl, G. *J. Phys. Chem*. **1999**, *103*, 6267.
(19) Over, H.; Kim, Y. D.; Seitsonen, A. P.; Wendt, S.; Lundgren, E.; Schmid, M.; Varga, P.; Morgante, A.; Ertl, G. *Science* **2000**, *287*, 1474.
(20) Hadzi-Jordanov, S.; Angerstein-Kozlowska, H.; Vukovic, M.; Conway, B. E. *J. Electrochem. Soc*. **1978**, *125*, 1471.
(21) Kötz, R.; Lewerenz, H.-J.; Stucki, S. *J. Electrochem. Soc*. **1983**, *130*, 825.
(22) Chan, H. Y. H.; Takoudis, C. G.; Weaver, M. J. *J. Catal*. **1997**, *172*, 336.
(23) Trasatti, S. In *Interfacial Electrochemistry*; Wieckowski, A., Ed.; Marcel Dekker: New York, 1999; p 769.
(24) Lezna, R. O.; De Tacconi, N. R.; Arvia, A. J. *J. Electroanal. Chem*. **1983**, *151*, 193.
(25) (a) Burke, L. D.; Mulcahy, J. K. *J. Electroanal. Chem*. **1976**, *73*, 207. (b) Burke, L. D.; Mulcahy, J. K.; Venkatesan, S. *J. Electroanal. Chem*. **1977**, *81*, 339.

(26) Birss, V.; Myers, R.; Angerstein-Kozlowska, H.; Conway, B. E. *J. Electrochem. Soc.* **1984**, *131*, 1502.
(27) Vukovic, M.; Valla, T.; Milun, M. *J. Electroanal. Chem.* **1993**, *356*, 81.
(28) Michell, D.; Rand, D. A. J.; Woods, R. *J. Electroanal. Chem.* **1978**, *89*, 11.
(29) Kinoshita, K., Ross, P. N. *J. Electroanal. Chem.* **1977**, *78*, 313.
(30) Cao, E. Y.; Stern, D. A.; Gui, J. Y.; Hubbard, A. T. *J. Electroanal. Chem.* **1993**, *354*, 71 and references therein.
(31) Zavadil, K. R.; Ingersoll, D.; Rogers, J. W., Jr. *J. Electroanal. Chem.* **1991**, *318*, 223.
(32) Wu, K.; Zei, M. S. *Surf. Sci.* **1998**, *415*, 212.
(33) Lin, W. F.; Zei, M. S.; Eiswirth, M.; Ertl, G.; Iwasita, T.; Vielstich, W. *J. Phys. Chem. B* **1999**, *103*, 6968.
(34) Over, H.; Bludau, H.; Skottke-Klein, M.; Moritz, W.; Ertl, G. *Phys. Rev. B* **1992**, *46*, 4360.
(35) Over, H.; Gierer, M.; Bludau, H.; Ertl, G.; Tong, S. Y. *Surf. Sci*. **1994**, *314*, 243.
(36) Aberdam, D.; Durand, R.; Faure, R.; El-Omar, F. *Surf. Sci*. **1986**, *171*, 303.
(37) Penckert, M.; Coenen, F. P.; Bonzel, H. P. *Electrochim. Acta* **1984**, *29*, 1305.
(38) Vogel, W. Private communication, Aug 1999.
(39) Conway, B. E. *Prog. Surf. Sci*. **1995**, *49*, 331.
(40) (a) Ryden, W. D.; Lawson, H. W. *Phys. Rev. B* **1970**, *1*, 1494. (b) Henrich, V. E.; Cox, P. A. *The Surface Science of Metal Oxides*; Cambridge University Press: Cambridge, U.K., 1996.
(41) Lu, P.; He, S.; Li, F. X.; Jia, Q. X. *Thin Solid Films* **1999**, *340*, 140.
(42) Kaga, Y.; Abe, Y.; Yanagisawa, H.; Sasaki, K. *Jpn. J. Appl. Phys*. **1998**, *37*, 3457.
(43) Meng, L.-J.; dos Santos, M. P. *Appl. Surf. Sci*. **1999**, *147*, 94.
(44) Maeder, T.; Muralt, P.; Sagalowicz, L. *Thin Solid Films* **1999**, *345*, 300.
(45) Kötz, R.; Stucki, S.; Scherson, D.; Kolb, D. M. *J. Electroanal. Chem.* **1984**, *172*, 211.